

Thinh-Phat Cao,^a Jin Myung Choi,^a Sang-Jae Lee,^b Yong-Jik Lee,^b Sung-Keun Lee,^c Youngsoo Jun,^d Dong-Woo Lee^b and Sung Haeng Lee^{a*}

^aDepartment of Cellular and Molecular Medicine, Chosun University School of Medicine, 375 Seo-suk dong, Gwangju 501-759, Republic of Korea,

^bSchool of Applied Biosciences, Kyungpook National University, Daegu 702-701, Republic of Korea, ^cDepartment of Pharmacology, College of Medicine, Inha University, Incheon 400-712, Republic of Korea, and

^dBio-Imaging and Cell Dynamics Research Center, School of Life Sciences, Gwangju Institute of Science and Technology, Gwangju 500-712, Republic of Korea

Correspondence e-mail: sunglee@chosun.ac.kr

Received 25 September 2013

Accepted 12 December 2013



© 2014 International Union of Crystallography
All rights reserved

Crystallization and preliminary X-ray crystallographic analysis of L-arabinose isomerase from thermophilic *Geobacillus kaustophilus*

L-Arabinose isomerase (AI), which catalyzes the isomerization of L-arabinose to L-ribulose, can also convert D-galactose to D-tagatose, a natural sugar replacer, which is of commercial interest in the food and healthcare industries. Intriguingly, mesophilic and thermophilic AIs showed different substrate preferences and metal requirements in catalysis and different thermostabilities. However, the catalytic mechanism of thermophilic AIs still remains unclear. Therefore, thermophilic *Geobacillus kaustophilus* AI (GKAI) was over-expressed, purified and crystallized, and a preliminary X-ray diffraction data set was obtained. Diffraction data were collected from a GKAI crystal to 2.70 Å resolution. The crystal belonged to the monoclinic space group *C*2, with unit-cell parameters $a = 224.12$, $b = 152.95$, $c = 91.28$ Å, $\beta = 103.61^\circ$. The asymmetric unit contained six molecules, with a calculated Matthews coefficient of $2.25 \text{ \AA}^3 \text{ Da}^{-1}$ and a solvent content of 45.39%. The three-dimensional structure determination of GKAI is currently in progress by molecular replacement and model building.

1. Introduction

L-Arabinose isomerase (AI; EC 5.3.1.4) was first observed and described by Lampen (Simpson & Wood, 1958) in *Lactobacillus pentosus* grown on L-arabinose. AI, encoded by the *araA* gene of the arabinose operon, catalyzes the reversible isomerization of L-arabinose to L-ribulose as the first step of the catabolism of L-arabinose to xylulose 5-phosphate, an intermediate in the pentose phosphate pathway (Schleif, 2010; Simpson *et al.*, 1958; Wolin *et al.*, 1958). Recently, AI has been exploited as an industrial enzyme for the production of D-tagatose as a sugar substitute in the food industry (Cheetham & Wootten, 1993; Lee *et al.*, 2004; Kim *et al.*, 2002; Oh, 2007). Owing to the structural similarity of its substrates, which may be explained by their sharing a hydroxyl group at C₃–C₄ in a *cis* configuration, AI can also catalyze the isomerization of D-galactose to D-tagatose (Cheetham & Wootten, 1993; Izumori *et al.*, 1978).

D-Tagatose, a natural ketohexose, has been considered not only as a potential sugar substitute in foods and beverages, but also as an additive in pharmaceutical and cosmetic formulas (Lee *et al.*, 2004; Levin *et al.*, 1995). Previously, calcium catalysts have been used to produce D-tagatose from D-galactose derived from lactose hydrolysis (Beadle *et al.*, 1992), but this chemical process has some defects with respect to byproduct formation and the production of environmental chemical waste. An alternative, biological conversion of D-galactose to D-tagatose using AI would be advantageous with respect to the feasibility of the process and the production yield (Cheetham & Wootten, 1993; Lee *et al.*, 2004). Initially, mesophilic AIs from *Escherichia coli* (ECAI) and *Lactobacillus gayonii* were examined for the production of D-tagatose (Cheetham & Wootten, 1993; Roh *et al.*, 2000). However, when mesophilic AIs were used, they showed very low conversion yields, which were not sufficient to meet industrial demands. For this reason, hyperthermophilic AIs derived from *Thermotoga neapolitana*, *T. maritima* and *Thermoanaerobacter mathranii* appear to be suitable for industrial applications (Lee *et al.*, 2004; Jørgensen *et al.*, 2004; Kim *et al.*, 2002). Indeed, those enzymes would be the best candidates for high yields of D-tagatose production. *T. neapolitana* AI (TNAI) exhibited isomerization activity of D-galactose to D-tagatose with a high yield of 68% conversion at

353 K in the presence of divalent metal ions such as Co^{2+} or Mn^{2+} (Kim *et al.*, 2002). In addition, another hyperthermophilic AI from *T. maritima* (TMAI), which has 94.8% amino-acid sequence identity to TNAI, showed very similar physicochemical properties, with a high d-tagatose conversion yield ($\geq 56\%$) from d-galactose at 353 K in the presence of Co^{2+} or Mn^{2+} (Lee *et al.*, 2004). Intriguingly, in contrast to mesophilic AIs, (hyper)thermophilic AIs have a strong metal dependence of their catalytic activity and structural stability (Lee, Hong *et al.*, 2005; Lee, Choe *et al.*, 2005). A recent mutational study using chimeric AIs showed that the metal-dependent catalytic activity and thermostability at elevated temperatures might be ascribed to structurally region-specific evolution (Hong *et al.*, 2011). For these and related reasons, the three-dimensional structures of AIs from (hyper)thermophiles will provide insights into the molecular basis of the distinct catalytic activity and thermostability of thermostable AIs over their mesophilic counterparts. However, no three-dimensional structure of an AI is available apart from that of the mesophilic *E. coli* AI (ECAI), which contains a trimeric architecture in the asymmetric unit (Manjasetty & Chance, 2006).

In this study, we chose a thermostable AI (GKAI) from the thermophilic *Geobacillus kaustophilus* which can grow optimally at 333 K (Takami *et al.*, 1997, 2004; Nazina *et al.*, 2001). The monomeric AI from *G. kaustophilus* (GKAI) consists of 497 amino-acid residues with a predicted molecular weight of ~ 56.2 kDa and a pI value of 5.42. As described above, in order to investigate the molecular basis of the thermostability and substrate specificity of thermophilic AIs in comparison with mesophilic AIs, we expressed the *araA* gene from *G. kaustophilus* in *E. coli*, purified the recombinant GKAI, crystallized it and performed preliminary crystallographic analysis to obtain the three-dimensional structure of GKAI.

2. Materials and methods

2.1. Cloning and protein expression of the *araA* gene

In a search of microbial genome sequences in GenBank, we identified a putative *araA* gene (NCBI Gene ID 3185813) from *G. kaustophilus*. The bacterial strain was purchased from the Korean Culture Type Collection (KCTC) and its genomic DNA was isolated using a genomic DNA extraction kit (Qiagen, Germany) according to

the manufacturer's instructions. The *araA* gene was amplified by PCR using the oligonucleotide primers 5'-CATATGATGCTGTCATTACGTCCCTTATGAA-3' (forward) and 5'-AAGCTTTACCGCCCCCGC-3' (reverse). The PCR primers were designed to include *Nde*I and *Hind*III restriction sites in the forward and reverse primers for cloning into pET-15b(+). PCR was performed in 1× PCR buffer consisting of 2 mM MgCl₂, 20 ng DNA, 10 pmol primers, 200 μ M dNTP mix, 2.5 U Ex Taq DNA polymerase (Takara, Japan) in a total volume of 50 μ l. After an initial denaturation for 4 min at 367 K, the DNA was amplified for 30 cycles (30 s denaturation at 367 K, 30 s annealing at 333 K and 1 min extension at 345 K), followed by a final extension step of 5 min at 345 K. The PCR product was cloned into the pGEM-T Easy vector and transformed into *E. coli* DH5 α . Transformants were selected on LB-ampicillin plates containing 0.01% 5-bromo-4-chloro-3-indolyl- β -D-galactopyranoside (X-Gal). The nucleotide sequence of clones with inserts was confirmed by sequencing and the plasmid DNA was subsequently digested with *Nde*I and *Hind*III flanking the multiple cloning sites of the expression vector pET-15b(+). The *araA* gene of *G. kaustophilus* was ligated into the *Nde*I and *Hind*III sites of pET-15b(+), yielding pET15b(+)-GKAI. The expression vector was transformed into *E. coli* BL21 (DE3). The resulting recombinant DNA in the expression vector contained a hexahistidine (6 \times His) tag and thrombin cleavage site at the N-terminus. For expression of the recombinant enzymes, the transformed *E. coli* BL21 (DE3) cells were grown in 1 l LB medium at 310 K containing 100 μ g ml⁻¹ ampicillin, induced in the mid-exponential phase ($\text{OD}_{600} = 0.6$) with 1 mM isopropyl- β -D-1-thiogalactopyranoside (IPTG), grown for an additional 5 h and harvested by centrifugation (5000 g for 20 min at 277 K).

2.2. Purification of GKAI

Bacterial cells (1 l culture) expressing 6 \times His-tagged GKAI were resuspended in 25 ml lysis buffer (20 mM Tris-HCl pH 7.5) containing 500 mM NaCl, 10 mM imidazole, 1 mM PMSF and protease-inhibitor cocktail tablet (Roche, Germany) and then disrupted by sonication. The lysate was centrifuged at 20 000 g for 30 min and the supernatant was heated at 333 K for 20 min and then centrifuged at 20 000 g for 30 min to remove the denatured *E. coli* proteins (Fig. 1a). The resulting supernatant from both cases was passed through a 0.4 μ m filter (Sartorius, Germany) and loaded onto

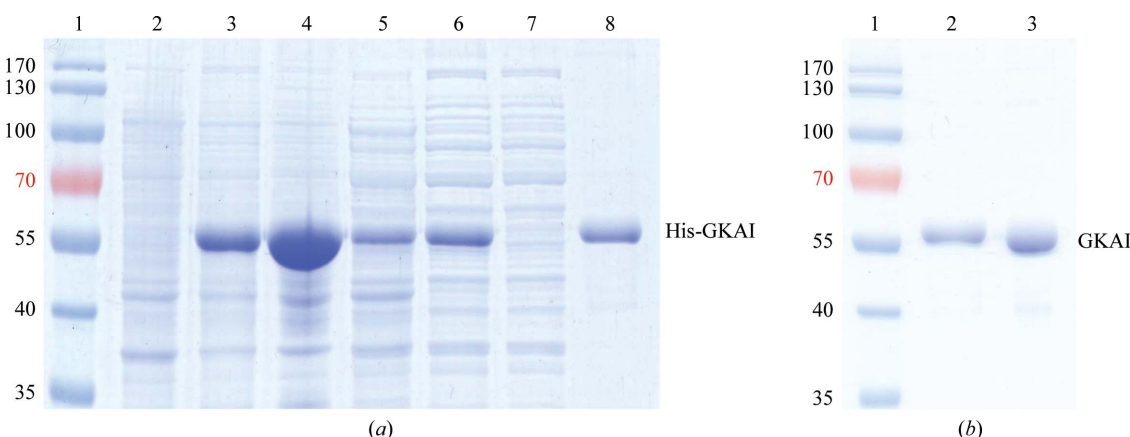


Figure 1

SDS-PAGE analysis of purified 6 \times His-tagged GKAI (a) and intact GKAI (b). (a) The bacterial lysate and purified recombinant fusion proteins were analyzed using 12% SDS-PAGE. Lane 1, molecular-mass markers (labelled in kDa); lane 2, lysate from non-induced cells; lane 3, lysate from induced cells; lane 4, pellets from induced cells; lane 5, supernatant (soluble fraction) from induced cells; lane 6, supernatant after heat treatment at 333 K for 20 min; lane 7, unbound fractions from the Ni-NTA agarose column; lane 8, purified 6 \times His-tagged GKAI. (b) The extra 17 amino acids including the 6 \times His tag were removed by thrombin digestion. The resulting molecular mass is approximately 2 kDa lower than that of the fusion protein. Lane 1, molecular-mass markers (labelled in kDa); lane 2, 6 \times His-tagged GKAI (~ 58 kDa); lane 3, thrombin-digested GKAI (~ 56 kDa).

an Ni–NTA agarose affinity column (1.5 ml; Qiagen, Germany). The column was then washed with 20 mM Tris–HCl pH 7.5 buffer containing 0.5 M NaCl, 20 mM imidazole and the His-tagged protein was eluted using 250 mM imidazole in the lysis buffer (Fig. 1a). To remove the His tag from the fusion protein using thrombin, we exchanged the buffer system by dialyzing against 20 mM Tris–HCl pH 7.5 buffer containing 150 mM NaCl. Seven units of thrombin protease (HTI, USA) were added to the dialyzed fusion protein (\sim 10 mg) for 1 h to yield intact GKAI without any 6 \times His. After that, the GKAI was subjected to size-exclusion chromatography on a HiLoad 16/600 Superdex 200 pg column (GE Healthcare, USA) pre-equilibrated with 20 mM Tris–HCl pH 7.5, 50 mM NaCl. The major peak fractions were collected, analyzed by SDS–PAGE and visualized with Coomassie Blue (Fig. 1b).

AI activity was assayed by measuring the increase in L-ribulose as described previously (Lee, Hong *et al.*, 2005). L-Ribulose was quantified by the cysteine–sulfuric acid–carbazole method and the absorbance was measured at 560 nm. One unit of isomerase activity is defined as the amount of enzyme that produces 1 μ mol of product per minute under the assay conditions.

2.3. Crystallization of GKAI

Metal ions were removed from the purified GKAI by treatment with 10 mM EDTA at 333 K for 1 h followed by overnight dialysis against 20 mM Tris–HCl buffer pH 7.5, 50 mM NaCl at 277 K with several changes of buffer. The divalent metal contents of the as-isolated and EDTA-treated samples were determined by high-resolution inductively coupled plasma (ICP) mass spectrometry on a PlasmaQuad 3 instrument at the Korea Basic Science Institute, Kyungpook National University. The purified GKAI was concentrated to \sim 10 mg ml $^{-1}$ in 20 mM Tris buffer pH 7.5, 50 mM NaCl with or without 0.5 mM Mn $^{2+}$. Crystallization conditions for GKAI were extensively screened using commercial solutions from Hampton Research (Index, SaltRx, PEG/Ion, PEG/Ion 2, Crystal Screen, Crystal Screen 2 and Crystal Screen Lite), Emerald BioSystems (Wizard I, II, III and IV) and \sim 500 additional homemade solutions at 293 K. The preliminary crystallization of GKAI with and without Mn $^{2+}$ was carried out by the hanging-drop vapour-diffusion method in a drop consisting of 1 μ l protein solution and 1 μ l reservoir solution. Initially, several conditions, including Crystal Screen Lite conditions Nos. 14 and 23, SaltRx 2 condition No. 9, Wizard I



Figure 2

Crystals of GKAI. Crystals were grown in 1 M sodium citrate, 0.1 M imidazole pH 8.0 to dimensions of 0.02 \times 0.15 \times 0.4 mm for the rod-shaped crystals (indicated by arrows). Diffraction data were only obtained from the rod-shaped crystals; the thin hexagonal crystals (indicated by an asterisk) diffracted poorly.

Table 1

Crystallographic data-collection statistics for GKAI.

Values in parentheses are for the highest resolution shell.

Beamline	PAL-5C
Wavelength (Å)	0.97951
Temperature (K)	100
Space group	C2
Unit-cell parameters (Å, $^\circ$)	$a = 224.12, b = 152.95, c = 91.28, \alpha = 90.0, \beta = 103.61, \gamma = 90.0$
Resolution (Å)	50.0–2.7 (2.75–2.70)
Completeness (%)	99.2 (99.9)
Multiplicity	5.0 (5.0)
Total reflections	398560
Unique reflections	79807 (4031)
$R_{\text{merge}}^{\dagger}$ (%)	9.6 (48.0)
$R_{\text{meas}}^{\ddagger}$ (%)	11.5 (48.4)
Average $I/\sigma(I)$	15.289 (2.992)
Matthews coefficient (Å 3 Da $^{-1}$)	2.25
Solvent content (%)	45.39
No. of chains per asymmetric unit	6

$\dagger R_{\text{merge}} = \sum_{hkl} \sum_i |I_i(hkl) - \langle I(hkl) \rangle| / \sum_{hkl} \sum_i I_i(hkl)$, where $I_i(hkl)$ and $\langle I(hkl) \rangle$ are the intensity of an individual reflection and the mean value of all measurements of an individual reflection, respectively. $\ddagger R_{\text{meas}} = \sum_{hkl} \{N(hkl)/[N(hkl) - 1]\}^{1/2} \sum_i |I_i(hkl) - \langle I(hkl) \rangle| / \sum_{hkl} \sum_i I_i(hkl)$, where $N(hkl)$ is the number of observations of the reflection with index hkl and $I_i(hkl)$ is the intensity of its i th observation.

condition No. 36 and Wizard II condition No. 14, yielded tiny crystals within 2–5 d. Amongst these, Wizard I condition No. 36 generated well edged crystals of a suitable size (\sim 0.3 mm in length) for direct diffraction tests. We then tried to improve the size and quality of the crystals by varying the concentrations of salt, precipitants and protein and the pH value around each original solution. However, even after improvement trials, we finally found better crystals for X-ray diffraction from the original Wizard I condition No. 36 (0.1 M imidazole hydrochloric acid pH 8.0, 1 M sodium citrate tribasic). In this condition, stick-like crystals were obtained with dimensions of 0.02 \times 0.15 \times 0.4 mm in a week (Fig. 2). After screening several cryoprotectants including glycerol, 2-methyl-2,4-pentanediol (MPD) and polyethylene glycol, the crystals were found to be stable in the presence of 30% (w/v) glycerol. The crystals were picked up in a nylon loop and then soaked for 30–60 s in a solution consisting of 0.1 M imidazole–HCl pH 8.0, 1 M sodium citrate tribasic, 30% (w/v) glycerol and flash-cooled in liquid nitrogen for synchrotron-radiation diffraction.

2.4. Diffraction experiments

Crystals were mounted in stream of cold nitrogen (100 K). X-ray diffraction data were collected on beamline PAL-5C at the Pohang Light Source (Pohang, Republic of Korea) using an ADSC Quantum 315 CCD detector, an oscillation of 1.0° and 5 s exposure per frame over a 360° range at a wavelength of 0.97951 Å (Fig. 3). During diffraction, the crystals diffracted to a maximum resolution of 2.70 Å. The diffraction data sets were indexed and scaled with HKL-2000 (Otwinowski & Minor, 1997) and the diffraction statistics are shown in Table 1. The initial structure solution was determined by molecular replacement using the CCP4 program MOLREP and the structure of AI from *E. coli* as a search model (PDB entry 2ajt; Manjasetty & Chancé, 2006). Model building and refinement are in progress with Coot (Emsley & Cowtan, 2004) and PHENIX (Adams *et al.*, 2002).

3. Results and discussion

Although AIs from (hyper)thermophilic bacteria are attractive options for the commercial production of D-tagatose from D-galactose, their substrate specificities are directly correlated with their conver-

sion efficiency, which needs to be further improved through protein engineering to give a cost-effective biological process. Thus, we attempted to determine the three-dimensional structure of AI from the thermophilic *G. kaustophilus*. The *araA* gene encoding AI (amino acids 1–497) was cloned into an expression plasmid conferring an N-terminal 6×His affinity tag. The constructed plasmid was transformed into *E. coli* BL21 (DE3) cells for overexpression of GKAI. Consequently, a significant amount of His-fused GKAI was successfully obtained as a soluble form with the expected molecular weight of ~58 kDa, including N-terminal extra residues corresponding to a 6×His tag and thrombin cleavage site, although more than 80% of the total expressed protein was produced as inclusion bodies (Fig. 1a, lanes 3–5). GKAI in the soluble fraction (Fig. 1a, lane 5) exhibited enzyme activity for the isomerization of L-arabinose to L-ribulose at 333 K, but the inclusion bodies did not, indicating that soluble GKAI exists in an active and stable conformation. Indeed, even after heat treatment at 333 K for 20 min (Fig. 1a, lane 6), a significant amount of recombinant GKAI in the soluble fraction retained its isomerization activity, suggesting that the soluble 6×His GKAI in *E. coli* might retain a stable conformation. The His-fused GKAI in the soluble fraction was successfully purified using Ni-NTA column chromatography (Fig. 1a, lanes 7 and 8), as was the case for other AIs from thermophilic *G. stearothermophilus* (GSAI) and hyperthermophilic *T. maritima* (TMAI) (Lee, Hong *et al.*, 2005; Hong *et al.*, 2011). The extra residues harbouring the 6×His tag and protease cleavage site at the N-terminus were thus successfully removed to generate intact 56 kDa GKAI (Fig. 1b), suggesting that the protease cleavage site is appropriately exposed to thrombin when the thermophilic AI is folded in *E. coli*. This was supported by the fact that the recombinant GKAI retained its isomerization activity (4.57 ± 0.08 U mg⁻¹) for L-arabinose as a substrate at 333 K. Therefore, the recombinant GKAI was suitable for use in crystallization trials.

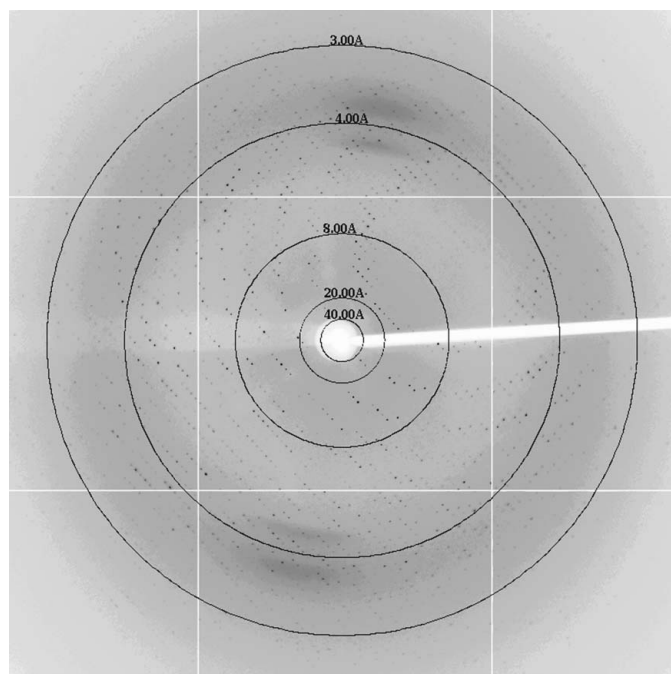


Figure 3

A diffraction image of a GKAI crystal. The diffraction data were collected from a single cryocooled GKAI crystal with a crystal-to-detector distance of 310 mm using a wavelength of 0.97951 Å. The oscillation was 1.0° per frame with 5 s exposure over a 320° range; the edge of the detector corresponds to 2.7 Å resolution.

Amongst the screening-reagent kits listed above, there were two major conditions that produced GKAI crystals: SaltRx 2 condition No. 9 (1.8 M sodium phosphate monobasic, potassium phosphate dibasic pH 6.9) and Wizard I condition No. 36 (1 M sodium citrate, 0.1 M imidazole pH 8.0). Initially, crystals from SaltRx 2 condition No. 9 were smaller and relatively amorphous compared with those from the other condition and did not seem to be appropriate for diffraction trials. However, the crystals from Wizard I condition No. 36 were suitable for direct use in diffraction tests. Although we attempted to improve the quality of the crystals further with a variety of salt concentrations and solution pH values from the above two conditions, crystals from the original composition of Wizard I condition No. 36 finally provided the best diffraction data (Table 1).

Although the amino-acid sequences of mesophilic and thermophilic AIs are quite similar (>80%), their physicochemical properties are quite different (Hong *et al.*, 2011). As described above, in contrast to mesophilic AIs, the activity of which has little metal dependence, thermophilic AIs depend on divalent metal ions such as Mn²⁺ or Co²⁺ for their catalytic activity and thermostability. Previous reports have proposed that such distinct properties between mesophilic and thermophilic AIs might be attributed to a marginal contribution in a region-specific manner (Lee, Lee *et al.*, 2005; Hong *et al.*, 2011; Lee *et al.*, 2012). In this regard, in order to obtain an insight into the molecular and structural basis of such metal-dependent distinct properties using GKAI, we screened crystallization conditions for GKAI with and without Mn²⁺. To obtain the apoenzyme ($<0.003 \pm 0.0002$ Mn²⁺ ions per monomer by ICP mass spectrometry), the purified enzyme (as isolated) was treated with 10 mM EDTA for 1 h at 333 K, followed by dialysis against 20 mM Tris-HCl buffer pH 7.5 overnight with several changes of buffer. Remarkably, apo GKAI showed very little activity (0.84 ± 0.02 U mg⁻¹ at 333 K), whereas the enzyme showed significantly increased activity (4.03 ± 0.13 U mg⁻¹ at 333 K) in the presence of 1 mM Mn²⁺, as was the case for AI from thermophilic *G. stearothermophilus* (Lee, Choe *et al.*, 2005).

A crystallization condition consisting of 1 M sodium citrate, 0.1 M imidazole pH 8.0 finally produced two crystal morphologies (long rod shape and thin hexagonal plates) in the same drop regardless of the presence of Mn²⁺ (Fig. 2). The rod-shaped crystal diffracted to 2.7 Å resolution (Fig. 3), whereas the hexagonal crystal diffracted very poorly (~7 Å) and was too fragile to handle. Therefore, we chose the rod-shaped crystal to obtain diffraction data for GKAI. Based on autoindexing and scaling using HKL-2000, the crystal belonged to space group C2, with unit-cell parameters $a = 224.12$, $b = 152.95$, $c = 91.28$ Å, $\beta = 103.61^\circ$ (Table 1). A total of 398 560 reflections were measured in the resolution range 50.0–2.7 Å. The asymmetric unit is likely to contain six GKAI molecules, corresponding to a calculated Matthews coefficient of 2.25 Å³ Da⁻¹ and a solvent content of 45.39% (Matthews, 1968). Previously, biophysical and electron-microscopy studies demonstrated that native ECAI exists as a homohexamer complex in solution (Pauley *et al.*, 1972; Wallace *et al.*, 1978), while thermostable AIs mostly exhibit homotetramers as described in Lee *et al.* (2004), Jørgensen *et al.* (2004) and Manjasetty & Chance (2006). However, our analytical size-exclusion chromatography revealed that the purified GKAI in this study has a hexameric structure (~321 kDa), which correlated well with the predicted molecular weight (~336 kDa) of the homohexameric complex. The crystal structure of GKAI therefore also needs to be thoroughly investigated in order to elucidate these differences as well as the metal-dependent catalytic efficiency at elevated temperatures. We attempted to solve the structure by molecular replacement using the single chain of *E. coli* AI as a search model (PDB entry 2ajt; Manjasetty & Chance, 2006), which exhibits high levels of sequence

identity and similarity of 61 and 75%, respectively, to GKAI. With a good molecular-replacement solution, an initial round of crystallographic refinement was carried out using rigid-body refinement, resulting in convergence to an *R* factor of 28.37% and an *R*_{free} of 37.38% with six chains of GKAI in the asymmetric unit. This result also correlated with the expected number of chains in an asymmetric unit from the calculated Matthews coefficient. Further refinement is currently in progress to complete the quaternary structure of GKAI.

This study was supported in part by National Research Foundation (NRF) grants 2009-0064846 and 2010-0005114 (SHL) and Kyungpook National Research Fund (2013) (DWL). The authors thank the staff of beamline 5C of the Pohang Light Source (PLS), Pohang, Republic of Korea for support and help during data collection.

References

- Adams, P. D., Grosse-Kunstleve, R. W., Hung, L.-W., Ioerger, T. R., McCoy, A. J., Moriarty, N. W., Read, R. J., Sacchettini, J. C., Sauter, N. K. & Terwilliger, T. C. (2002). *Acta Cryst. D* **58**, 1948–1954.
- Beadle, J. R., Saunders, J. P., Thomas, J. & Wajda, J. (1992). US Patent 5215591.
- Cheetham, P. S. J. & Wootton, A. N. (1993). *Enzyme Microb. Technol.* **15**, 105–108.
- Emsley, P. & Cowtan, K. (2004). *Acta Cryst. D* **60**, 2126–2132.
- Hong, Y.-H., Lee, D.-W., Pyun, Y.-R. & Lee, S. H. (2011). *J. Agric. Food Chem.* **59**, 12939–12947.
- Izumori, K., Ueda, Y. & Yamanaka, K. (1978). *J. Bacteriol.* **133**, 413–414.
- Jørgensen, F., Hansen, O. C. & Stougaard, P. (2004). *Appl. Microbiol. Biotechnol.* **64**, 816–822.
- Kim, B.-C., Lee, Y.-H., Lee, H.-S., Lee, D.-W., Choe, E.-A. & Pyun, Y.-R. (2002). *FEMS Microbiol. Lett.* **212**, 121–126.
- Lee, D.-W., Choe, E.-A., Kim, S.-B., Eom, S.-H., Hong, Y.-H., Lee, S.-J., Lee, H.-S., Lee, D.-Y. & Pyun, Y.-R. (2005). *Arch. Biochem. Biophys.* **434**, 333–343.
- Lee, D.-W., Hong, Y.-H., Choe, E.-A., Lee, S.-J., Kim, S.-B., Lee, H.-S., Oh, J.-W., Shin, H.-H. & Pyun, Y.-R. (2005). *FEBS Lett.* **579**, 1261–1266.
- Lee, D.-W., Jang, H.-J., Choe, E.-A., Kim, B.-C., Lee, S.-J., Kim, S.-B., Hong, Y.-H. & Pyun, Y.-R. (2004). *Appl. Environ. Microbiol.* **70**, 1397–1404.
- Lee, S.-J., Lee, D.-W., Choe, E.-A., Hong, Y.-H., Kim, S.-B., Kim, B.-C. & Pyun, Y.-R. (2005). *Appl. Environ. Microbiol.* **71**, 7888–7896.
- Lee, S.-J., Lee, S. J., Lee, Y.-J., Kim, S.-B., Kim, S.-K. & Lee, D.-W. (2012). *Appl. Environ. Microbiol.* **78**, 8813–8816.
- Levin, G. V., Zehner, L. R., Saunders, J. P. & Beadle, J. R. (1995). *Am. J. Clin. Nutr.* **62**, 1161–1168.
- Manjasetty, B. A. & Chance, M. R. (2006). *J. Mol. Biol.* **360**, 297–309.
- Matthews, B. W. (1968). *J. Mol. Biol.* **33**, 491–497.
- Nazina, T. N., Tourova, T. P., Poltaraus, A. B., Novikova, E. V., Grigoryan, A. A., Ivanova, A. E., Lysenko, A. M., Petrunyaka, V. V., Osipov, G. A., Belyaev, S. S. & Ivanov, M. V. (2001). *Int. J. Syst. Evol. Microbiol.* **51**, 433–446.
- Oh, D.-K. (2007). *Appl. Microbiol. Biotechnol.* **76**, 1–8.
- Otwowski, Z. & Minor, W. (1997). *Methods Enzymol.* **276**, 307–326.
- Pauley, J., Power, J. & Irr, J. (1972). *J. Bacteriol.* **112**, 1247–1253.
- Roh, H. J., Kim, P., Park, Y. C. & Choi, J. H. (2000). *Biotechnol. Appl. Biochem.* **31**, 1–4.
- Schleif, R. (2010). *FEMS Microbiol. Rev.* **34**, 779–796.
- Simpson, F. J., Wolin, M. J. & Wood, W. A. (1958). *J. Biol. Chem.* **230**, 457–472.
- Simpson, F. J. & Wood, W. A. (1958). *J. Biol. Chem.* **230**, 473–486.
- Takami, H., Inoue, A., Fuji, F. & Horikoshi, K. (1997). *FEMS Microbiol. Lett.* **152**, 279–285.
- Takami, H., Takaki, Y., Chee, G.-J., Nishi, S., Shimamura, S., Suzuki, H., Matsui, S. & Uchiyama, I. (2004). *Nucleic Acids Res.* **32**, 6292–6303.
- Wallace, L. J., Eiserling, F. A. & Wilcox, G. (1978). *J. Biol. Chem.* **253**, 3717–3720.
- Wolin, M. J., Simpson, F. J. & Wood, W. A. (1958). *J. Biol. Chem.* **232**, 559–575.